Journal of Computational Physics 227 (2008) 9697–9710

Contents lists available at ScienceDirect

Journal of Computational Physics

journal homepage: www.elsevier.com/locate/jcp

Time step restrictions for Runge–Kutta discontinuous Galerkin methods on triangular grids

Ethan J. Kubatko [a,*], Clint Dawson [b], Joannes J. Westerink [c]

[a] Department of Civil and Environmental Engineering and Geodetic Science, The Ohio State University, Columbus, OH 43210, United States
[b] Institute for Computational Engineering and Sciences, The University of Texas at Austin, Austin, TX 78712, United States
[c] Department of Civil Engineering and Geological Sciences, University of Notre Dame, Notre Dame, IN 46556, United States

ARTICLE INFO

Article history:
Received 31 January 2008
Received in revised form 18 June 2008
Accepted 23 July 2008
Available online 19 August 2008

Keywords:
Discontinuous Galerkin
Strong-stability-preserving
Runge–Kutta

ABSTRACT

We derive CFL conditions for the linear stability of the so-called Runge–Kutta discontinuous Galerkin (RKDG) methods on triangular grids. Semidiscrete DG approximations using polynomials spaces of degree $p = 0, 1, 2$, and 3 are considered and discretized in time using a number of different strong-stability-preserving (SSP) Runge–Kutta time discretization methods. Two structured triangular grid configurations are analyzed for wave propagation in different directions. Approximate relations between the two-dimensional CFL conditions derived here and previously established one-dimensional conditions can be observed after defining an appropriate triangular grid parameter h and a constant that is dependent on the polynomial degree p of the DG spatial approximation. Numerical results verify the CFL conditions that are obtained, and "optimal", in terms of computational efficiency, two-dimensional RKDG methods of a given order are identified.

© 2008 Elsevier Inc. All rights reserved.

1. Introduction

Runge–Kutta discontinuous Galerkin (RKDG) methods are a widely used approach for the solution of time-dependent, hyperbolic and advection dominated advection–diffusion equations – see, for example, [1,2,5–9,14,19]. The methods have been used to model a wide range of physical phenomena such as gas dynamics, electromagnetics, shallow water flow, and advection of contaminants. Application of RKDG methods proceeds along the classical notions of the method of lines whereby the partial differential equation(s) (PDEs) are first discretized in space using a DG method, which produces a system of ordinary differential equations (ODEs), and then discretized in time using a special class of explicit RK time discretization methods. When using explicit methods it is well known that the grid spacing and the time step Δt that are employed must satisfy a CFL condition in order to guarantee stability.

For RKDG methods using DG spatial discretizations of polynomials of degree $p = k - 1$ and a k stage RK method of order k (such a method is referred to as a kth order RKDG method), Cockburn and Shu [9] give an approximate CFL condition for linear stability of the form:

$$|c|\frac{\Delta t}{\Delta x} \leqslant \frac{1}{2p+1}, \tag{1}$$

where $|c|$ is the wave speed associated with the given problem and Δx is the uniform grid spacing. This condition is, in fact, exact for the cases $p = 0$ and $p = 1$ (the case $p = 0$ can be proven trivially and the case $p = 1$ was proven in [7]). Furthermore,

* Corresponding author. Tel.: +1 614 292 7176.
E-mail address: kubatko.3@osu.edu (E.J. Kubatko).

0021-9991/$ - see front matter © 2008 Elsevier Inc. All rights reserved.
doi:10.1016/j.jcp.2008.07.026

for $p \geqslant 2$, this estimate was observed to be less than 5% smaller than numerically-obtained estimates of the CFL condition [9].

Given the somewhat restrictive nature of (1), especially as p increases, the stability of RKDG methods using so-called strong-stability-preserving (SSP) RK methods where the number of stages s is greater than the order k of the method were examined in [15] with the goal of obtaining more efficient RKDG methods. Necessary time step restrictions for stability were derived and "optimal" RKDG methods, in terms of computationally efficiency, were identified. For an RKDG method of a given order, the computational efficiency is a function of both the CFL condition and the number of stages of the SSP RK method. In the majority of cases examined in [15], use of the $s > k$ SSP RK methods was more efficient than the standard practice of using the $s = k$ methods. This was due to gains in allowable time step size afforded by improved CFL conditions for linear stability that were large enough to offset the additional work introduced by the increased number of stages. It was found that optimal RKDG methods were generally obtained by using one or two additional stages than theoretically required for a given order.

The work cited above has been for one-dimensional RKDG methods. In recent numerical experiments, we have noted that simple two-dimensional analogs of these CFL conditions do not appear to be sufficient for stability in two-dimensions on structured triangular grids. Therefore, in this paper, we seek to extend the types of one-dimensional analyses performed in [7,9,15] to RKDG methods in two-dimensions. Specifically, we derive necessary time step restrictions, which also appear to be sufficient, for the stability of RKDG methods on structured triangular grids applied to the constant coefficient, two-dimensional transport equation with periodic boundary conditions. Two different structured triangular grid patterns are examined on which we consider wave propagation in different directions. For these grids, the stability of RKDG methods of order $k = 1, 2, 3$, and 4 are considered. In the case of the first-order RKDG method, which is equivalent to a first-order finite volume method, CFL conditions are derived analytically by first constructing the semidiscrete DG equations over a repeating grid generation pattern, explicitly computing the eigenvalues of the resulting matrices, and then calculating the necessary restrictions so that, when scaled by the time step Δt, these eigenvalues lie within the stability region of a given RK method. For the first-order RKDG method, an exact relationship between the one- and two-dimensional CFL conditions is found once an appropriate triangular grid spacing parameter h is defined. For the higher-order methods, we use a semi-analytical approach in which the discrete equations are explicitly constructed as before but with the eigenvalues of the resulting matrices being computed numerically and then checked for the stability condition at a discrete number of points. In the high-order cases, approximate relationships between the one- and two-dimensional CFL conditions can be observed using the previously defined grid parameter h and a constant that is dependent on the polynomial degree p of the DG spatial discretization. The validity of these derived CFL conditions are demonstrated on numerical examples.

This paper is outlined as follows: First, in Section 2, we give a brief overview of the DG spatial discretization of the linear, two-dimensional transport equation using triangular elements, and we present the two structured, triangular grid patterns that will be considered in our stability analysis. Next, in Section 3, we review some aspects of RK time stepping methods that are pertinent to our objective of deriving CFL conditions. We begin by presenting the general form of the RK methods that are used and the so-called SSP theorem in Section 3.1 – noting some important facts related to this theorem that are specific to the application of SSP RK methods to the semidiscrete DG equations. This is followed by a brief overview of the stability of RK methods in Section 3.2. We then derive CFL conditions for RKDG methods using polynomials spaces of degree $p = 0, 1, 2$, and 3 and "matching order" SSP RK methods in Section 4. Several different SSP RK methods are examined, ranging from two to eight stages, and "optimal" two-dimensional RKDG methods, in terms of computational efficiency, are identified for a given order. This is followed by a brief subsection in which approximate relationships between the one- and two-dimensional RKDG CFL conditions are established. Finally, in Section 5, numerical results are presented that verify our stability analysis.

2. The discontinuous Galerkin spatial discretization

In this section, we consider the DG spatial discretization of the transient, two-dimensional, linear conservation law or transport equation over a domain $\Omega \subset \mathbb{R}^2$ with periodic boundary conditions:

$$\begin{aligned} &\frac{\partial u}{\partial t} + \nabla \cdot \mathbf{c}u = 0 \quad \text{in} \quad \Omega \times (0, T] \\ &u(x, y, 0) = u_0 \quad \text{on} \quad \Omega, \end{aligned} \tag{2}$$

with the vector $\mathbf{c} = \|\mathbf{c}\|(\cos\theta, \sin\theta)$ (assumed to be constant) where $\|\mathbf{c}\|$ and θ are the magnitude and direction of wave propagation, respectively, and u_0 is an initial condition.

Partitioning the domain Ω into a set of elements Ω_E, a weak formulation of the problem is obtained by multiplying Eq. (2) by a sufficiently smooth test function v and integrating by parts over each element:

$$\int_{\Omega_E} \frac{\partial u}{\partial t} v \, d\Omega - \int_{\Omega_E} \nabla v \cdot \mathbf{c} \, d\Omega + \int_{\Gamma_E} u\mathbf{c} \cdot \mathbf{n} v \, ds = 0,$$

where $\mathbf{n}$ denotes the outward unit normal vector of Γ_E the boundary of Ω_E.

Applying a DG method, the true solution u is approximated by $u_h \in U_h$ and the test function v is chosen such that $v = v_h \in U_h$ where U_h is the space $P^k(\Omega_E)$ of polynomials of degree k defined on Ω_E. Due to the fact that C^0 continuity is

not enforced between elements in the DG method, the flux $f = u\mathbf{c}\cdot\mathbf{n}$ along the boundaries Γ_E must be approximated by a numerical flux $\hat{f}$, which in the present case can be defined by upwinding:

$$\hat{f} = \begin{cases} u_h^-(\mathbf{c}\cdot\mathbf{n}_e) & \text{if} \quad \mathbf{c}\cdot\mathbf{n_e} \geqslant 0 \\ u_h^+(\mathbf{c}\cdot\mathbf{n}_e) & \text{if} \quad \mathbf{c}\cdot\mathbf{n_e} < 0, \end{cases}$$

where u_h^- and u_h^+ are the DG solution values computed on the $(-)$ and $(+)$ sides of the edge, respectively, as shown in Fig. 1, which is dictated by the orientation of the outward unit normal $\mathbf{n}_e$ of an edge e.

Thus, the discrete weak form of the problem takes the following form:

$$\int_{\Omega_E} \frac{\partial u_h}{\partial t} v_h \mathrm{d}\Omega - \int_{\Omega_E} \nabla v_h \cdot \mathbf{c}\mathrm{d}\Omega + \int_{\Gamma_E} \hat{f} v_h \mathrm{d}s = 0.$$

Insomuch as to define notation that will be used in Section 4, we note the following. The triangular elements Ω_E are mapped to a reference element $\widehat{\Omega}_E$ defined in a local coordinate system (ξ_1, ξ_2) as shown in Fig. 2. Using the inverse of this mapping, derivatives of the test functions v_h with respect to the (x, y) coordinates occurring in Eq. (2) can be computed via the equations:

$$\frac{\partial v_h}{\partial x} = \frac{1}{\Delta_E}\left[(y_3 - y_1)\frac{\partial v_h}{\partial \xi_1} + (y_1 - y_2)\frac{\partial v_h}{\partial \xi_2}\right]$$
$$\frac{\partial v_h}{\partial y} = \frac{1}{\Delta_E}\left[(x_1 - x_3)\frac{\partial v_h}{\partial \xi_1} + (x_2 - x_1)\frac{\partial v_h}{\partial \xi_2}\right],$$

where (x_1, y_1), (x_2, y_2), and (x_3, y_3) are the coordinates of the vertices of Ω_E numbered locally in a counter-clockwise manner and Δ_E is the area of element Ω_E. Related to these derivatives, we define the following elemental matrices and vectors:

$$\widehat{\mathbf{X}}_E = [\hat{\mathbf{x}}_E^{(1)}, \hat{\mathbf{x}}_E^{(2)}] = \frac{1}{\Delta_E}\begin{bmatrix} y_3 - y_1, & y_1 - y_2 \\ x_1 - x_3, & x_2 - x_1 \end{bmatrix}.$$

In what follows, we will derive time step restrictions necessary for the stability of the RKDG methods applied to Eq. (2) for the two structured grid configurations shown in Fig. 3, which can be thought of as being obtained by simply repeating the grid generation patterns shown in bold in block m, n. Grid pattern I consists of right isosceles triangles obtained by bisecting a square grid pattern to the left. Grid pattern II is made of equilateral triangles. Note also in Fig. 3 that we define the direction of propagation θ with respect to the x-axis (counterclockwise positive).

3. Runge–Kutta methods

In this section, we review some aspects of RK methods that are pertinent to the present analysis.

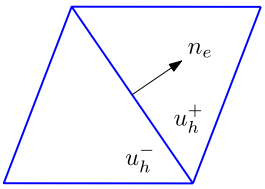

Fig. 1. The $(+)$ and $(-)$ sides of a given edge e.

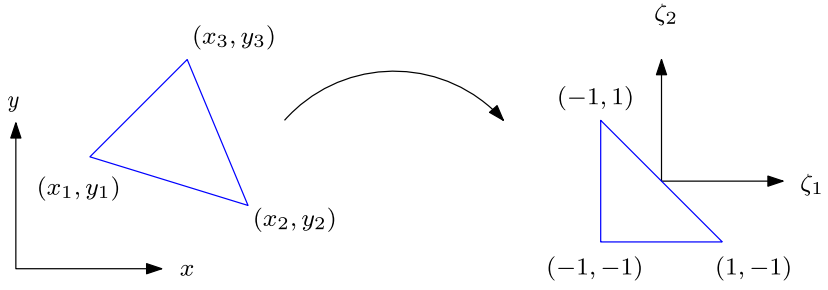

Fig. 2. Definition of the master element in the local (ζ_1, ζ_2) coordinate system.

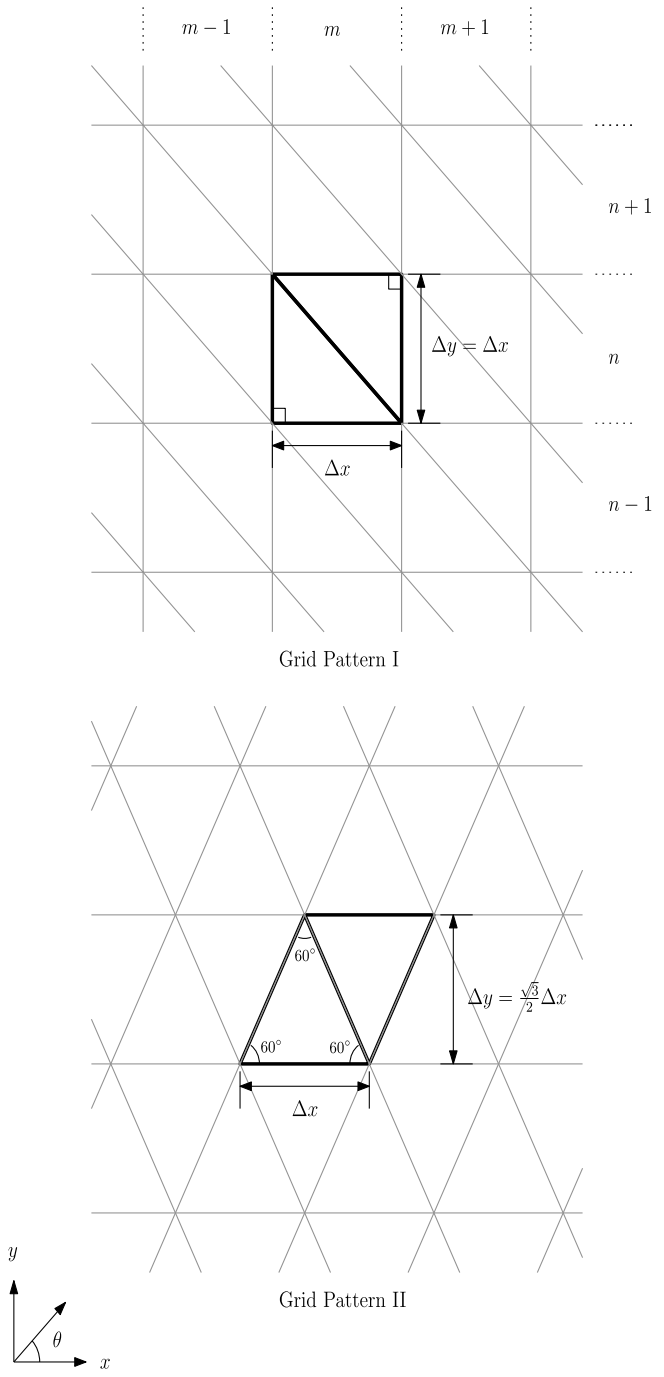

Fig. 3. The 2 grid configuration patterns considered in the stability analysis.

3.1. Strong-stability-preserving Runge–Kutta methods

Consider an explicit s-stage RK method written in the so-called Shu-Osher representation [20]:

$$\begin{aligned} u^{(0)} &= u^n \\ u^{(i)} &= \sum_{l=0}^{i-1} \{\alpha_{il} u^{(l)} + \Delta t \beta_{il} F(u^{(l)})\}, \quad i = 1, 2, \ldots, s \\ u^{n+1} &= u^{(s)}. \end{aligned} \tag{3}$$

If, in addition to the constraints placed on α_{il} and β_{il} relating to order (see, for example, [3]) and consistency ($\sum_{l=0}^{i-1}\alpha_{il}=1,\ i=1,2,\ldots,s$), the following additional constraints are enforced:

$$\begin{aligned}&\text{(i)}\alpha_{il}\geqslant 0 \quad \text{and} \quad \beta_{il}\geqslant 0\\ &\text{(ii)}\alpha_{il}=0 \quad \text{only if} \quad \beta_{il}=0,\end{aligned} \tag{4}$$

then the RK method can be written as a convex combination of forward Euler steps with time step sizes $\frac{\beta_{il}}{\alpha_{il}}\Delta t$, i.e.:

$$\begin{aligned}u^{(0)} &= u^n\\ u^{(i)} &= \sum_{l=0}^{i-1}\alpha_{il}\left\{u^{(l)}+\Delta t\frac{\beta_{il}}{\alpha_{il}}F(u^{(l)})\right\}, \quad i=1,2,\ldots,s\\ u^{n+1} &= u^{(s)}.\end{aligned}$$

Such a RK method is referred to as a strong-stability-preserving (SSP) RK method, the name being based on the following theorem (see, for example, [13]):

Theorem 1 (The SSP Theorem). *If the forward Euler method applied to the spatial discretization F is (strongly) stable in a given norm or semi-norm under the CFL condition $\Delta t\leqslant\Delta t_{FE}$ then the Runge–Kutta method (3) with constraints (4) preserves that stability under the CFL condition:*

$$\Delta t\leqslant\kappa\Delta t_{FE}, \tag{5}$$

where $\kappa\equiv\min_{i,l}(\frac{\alpha_{il}}{\beta_{il}})$ with $\frac{\alpha_{il}}{\beta_{il}}\equiv\infty$ for $\beta_{il}=0$.

Much of the research in the area of SSP methods has focused on finding optimal SSP RK methods – that is, the SSP RK method (5) for which κ is a maximum under the given constraints placed on the α_{il} and β_{il}, see, for example, [18].

It is interesting to note, however, that the SSP Theorem does not provide the criteria for linear (L^2) stability of the SSP RK methods applied to semidiscrete $p=k-1$ DG approximations with $k\geqslant 2$, due to the fact that for these cases the forward Euler method applied to the semidiscrete equations is unconditionally-unstable for a fixed Courant number $\nu\equiv c\Delta t/\Delta x$. This was proven explicitly for the case $k=2$ in [4], and the result carries over to all $p=k-1$ DG spatial discretizations for $k\geqslant 2$ [7]. Thus, in order to establish necessary time step restrictions for the linear stability of the RKDG methods the complete RK method must be analyzed. This is discussed in more detail in the next subsection.

The condition given in Theorem 1 does, however, play a role in the establishing the time step criteria necessary for the TVD (or TVB) property of the RKDG method (and also the linear stability of the $k=1$ RKDG case), since to establish the TVD (TVB) property of the RKDG methods a slope limiter is applied that renders the forward Euler method TV-stable under an appropriate CFL condition (see, for example, [9]). In two-dimensions, where enforcing the TVD property is incompatible with higher-order accuracy [11], a slope limiter can be applied to enforce a maximum principle when using the forward Euler method. The timestep restriction for TV-stability or enforcement of a maximum principle for a given SSP RK method is then provided by condition (5). However, in general, these conditions are much weaker than those required for linear stability, and, as pointed out in [9] and as demonstrated numerically in [15], it is the linear stability condition that must be respected or the high-order accuracy of the methods will degenerate to first-order. This fact prompted the investigation of the class of stage-exceeding-order (i.e. $s>k$) SSP RK methods applied to the semidiscrete DG equations presented in [15] in order to determine one-dimensional RKDG methods that are optimal in terms of computational efficiency, which is function of both the CFL conditions for linear stability and the number of stages of a given RK method. In all the cases examined in that work, optimal RKDG methods were obtained using RK methods with one or more additional stages than the order of the method. For this reason, the $s>k$ RK methods are also examined here in the two-dimensional setting.

3.2. The stability of Runge–Kutta methods

Associated with each s-stage, kth order RK method is a so-called characteristic polynomial $P_{s,k}$ obtained by applying the given RK method to the prototypical, scalar equation $\dot{u}=\lambda u$ where $\lambda\in\mathbb{C}$, which can be written in the form $u^{n+1}=P_{s,k}(z=\Delta t\lambda)u^n$. For example, the classic 2-stage, 2nd-order RK method (or modified Euler method) written in the Shu-Osher representation applied to this equation gives:

$$\begin{aligned}u^{(1)} &= u^n+zu^n\\ u^{n+1} &= \frac{1}{2}u^n+\frac{1}{2}u^{(1)}+\frac{1}{2}zu^{(1)}.\end{aligned}$$

Substituting $u^{(1)}$ into the equation for $u^{(n+1)}$ and simplifying gives:

$$u^{n+1}=\underbrace{\left(1+z+\frac{1}{2}z^2\right)}_{P_{2,2}(z)}u^n.$$

Thus, linear stability of the RK method is guaranteed provided:

$$|P_{s,k}(z)| \leqslant 1, \tag{6}$$

where $|\cdot|$ is the complex modulus $|x+\mathrm{i}y| = \sqrt{x^2+y^2}$ (x and y are real numbers and $i = \sqrt{-1}$). The set in the complex plane for which condition (6) is satisfied is the so-called region of absolute stability S of the given Runge–Kutta method, that is:

$$S = \{z : |P_{s,k}(z)| \leqslant 1|\}.$$

In terms of S then, condition (6) can be written as:

$$\Delta t\lambda \subseteq S. \tag{7}$$

In Fig. 4, we plot the regions of absolute stability for several of the SSP RK methods considered here where we have used the notation SSP (s,k) to denote an s stage, kth order SSP RK method.

In the case of applying an RK method to a system of equations, i.e. when the scalar λ in the equation considered above is replaced by a matrix $\mathbf{L}_h$, the issue of stability is a more delicate issue. If the matrix $\mathbf{L}_h$ is normal (see, for example, [22]) then stability is guaranteed if condition (7) holds for each eigenvalue λ of $\mathbf{L}_h$. In the general case, however, condition (7) is only a necessary, and not a sufficient, condition for stability. Necessary and sufficient conditions in the general (non-normal) case can be expressed in terms of the pseudospectra of $\mathbf{L}_h$, see, for example, [16]. Here, with the exception of the $k = 1$ RKDG case, we will content ourselves with finding necessary conditions according to (7). These conditions also appear to be sufficient as will be demonstrated in the numerical results section.

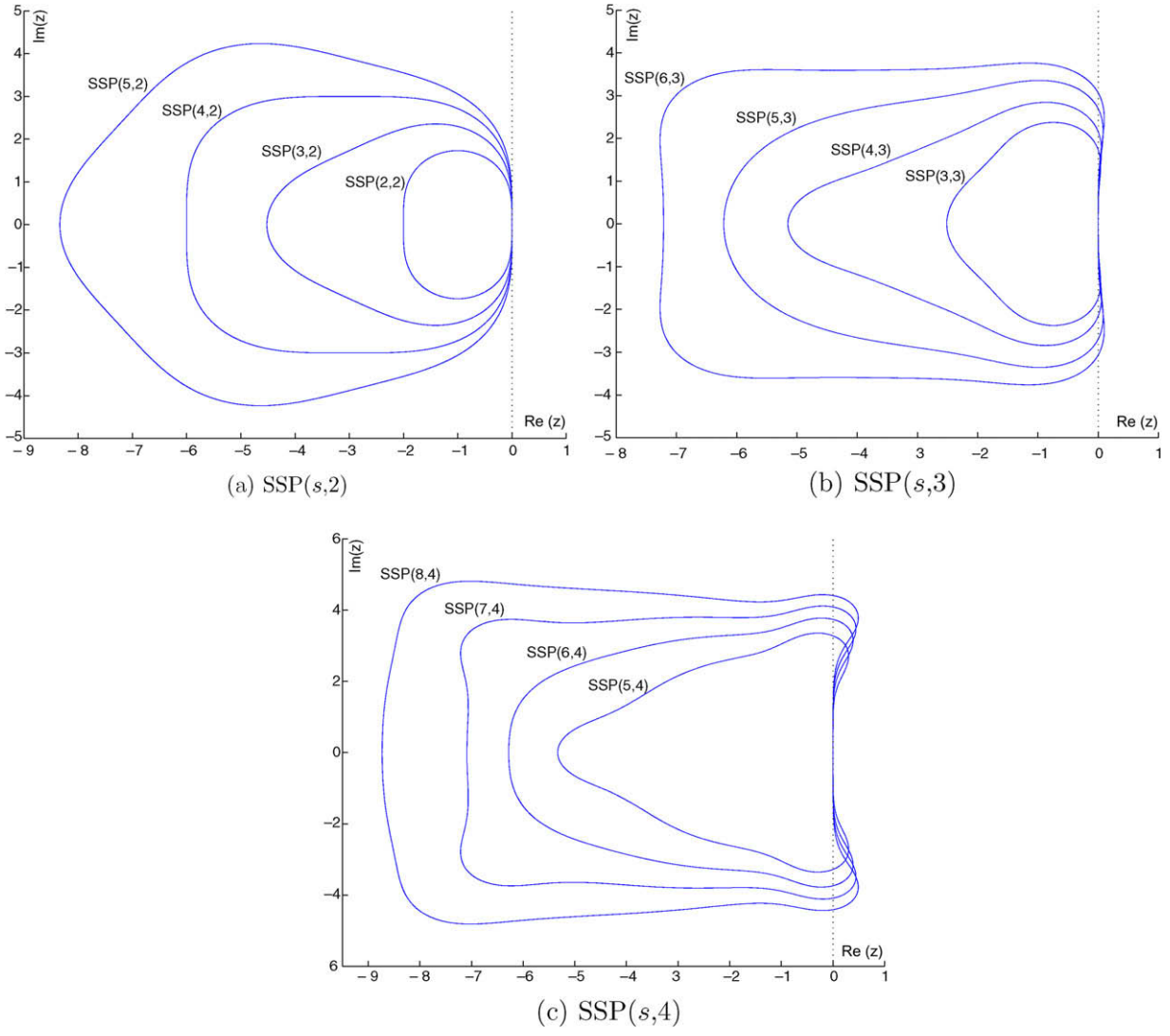

Fig. 4. Regions of absolute stability for the various SSP (s,k) RK methods.

4. Stability analysis

The discrete equations for the grid generation patterns shown in Fig. 3 can be written in the following compact form:

$$\mathbf{M}\frac{\mathrm{d}}{\mathrm{d}t}\mathbf{U}_{m,n} = \mathbf{A}\mathbf{U}_{m,n} - \mathbf{B}_{\pm}\mathbf{U}_{m\pm1,n} - \mathbf{C}_{\pm}\mathbf{U}_{m,n\pm1}, \tag{8}$$

where $\mathbf{U}_{m,n}$ is a vector containing the degrees of freedom for both of the elements in the grid block m,n (refer to Fig. 3), i.e.:

$$\mathbf{U}_{m,n} = \begin{bmatrix}\mathbf{u}_1\\ \mathbf{u}_2\end{bmatrix}.$$

Here $\mathbf{u}_1$ and $\mathbf{u}_2$ are vectors of length N_d containing the degrees of freedom of elements 1 and 2, respectively, of the given grid configuration ($N_\mathrm{d} = (p+1)(p+2)/2$ for a degree p triangular element). The mass matrix $\mathbf{M}$ is block diagonal:

$$\mathbf{M} = \begin{bmatrix}\mathbf{m}_1 & \mathbf{0}\\ \mathbf{0} & \mathbf{m}_2\end{bmatrix},$$

with blocks $\mathbf{m}_\mathrm{E}$, the elemental mass matrices, given by:

$$\mathbf{m}_\mathrm{E} = \frac{\Delta_\mathrm{E}}{2}\mathbf{m}, \quad m_{ij} = \int_{\widehat{\Omega}_\mathrm{E}} \phi_i\phi_j \mathrm{d}\widehat{\Omega}_\mathrm{E},$$

where m_{ij} is the ijth entry of the matrix $\mathbf{m}$.

The matrix $\mathbf{A}$ is made up of both elemental and edge contributions:

$$\mathbf{A} = \widehat{\mathbf{A}}_\mathrm{E} + \widetilde{\mathbf{A}}_\mathrm{e}.$$

The matrix $\widehat{\mathbf{A}}_\mathrm{E}$, like the mass matrix, is block diagonal with the blocks given by:

$$\hat{\mathbf{a}}_\mathrm{E} = \sum_{k=1}^{2}(\mathbf{c}\cdot\hat{\mathbf{x}}_\mathrm{E}^{(k)})\hat{\mathbf{a}}^{(k)}, \quad \hat{a}_{ij}^{(k)} = \int_{\widehat{\Omega}_\mathrm{e}} \frac{\partial\phi_i}{\partial\xi_k}\phi_j \mathrm{d}\widehat{\Omega}_\mathrm{E}.$$

The matrix $\widetilde{\mathbf{A}}_\mathrm{e}$ corresponds to contributions from the edge integrals that are interior to the grid generation pattern and the outflow edges on the boundary of the grid generation pattern. It is made up of blocks $\tilde{\mathbf{a}}_\mathrm{e}$:

$$\tilde{\mathbf{a}}_\mathrm{e} = \frac{l}{2}(\mathbf{c}\cdot\mathbf{n})\tilde{\mathbf{a}}, \quad \tilde{a}_{ij} = \int_\mathrm{e} \phi_i\phi_j \mathrm{d}s.$$

The matrices $\mathbf{B}$ and $\mathbf{C}$ are made up of the same blocks $\tilde{\mathbf{a}}_\mathrm{e}$, but corresponding to edges that are inflow edges on the boundary of the grid generation pattern. The structure of these matrices changes based on the wave propagation direction θ, which dictates the upwind direction. For example, the matrices of grid pattern I for $0 \leqslant \theta \leqslant \pi/2$ and grid pattern II for $0 \leqslant \theta \leqslant \pi/3$ will have the following structures:

$$\widetilde{\mathbf{A}}_\mathrm{e} = \begin{bmatrix}X, & 0\\ X, & X+X\end{bmatrix}, \quad \mathbf{B}_- = \begin{bmatrix}0, & X\\ 0, & 0\end{bmatrix}, \quad \mathbf{C}_- = \begin{bmatrix}0, & X\\ 0, & 0\end{bmatrix},$$

where the X's correspond to the matrices $\tilde{\mathbf{a}}_\mathrm{e}$ of a particular edge.

Following the ideas of classic Von Neumann stability analysis (see, for example, [17]), we seek a solution in the following form:

$$\mathbf{U}_{m,n} = \widehat{\mathbf{U}}_{m,n}\mathbf{e}^{\mathrm{i}(k_x m\Delta x + k_y n\Delta y)},$$

where k_x and k_y are wave numbers associated with the x and y directions, respectively. Substituting this into Eq. (8) and inverting the mass matrix, the following equation is obtained:

$$\frac{\mathrm{d}}{\mathrm{d}t}\widehat{\mathbf{U}}_{m,n} = \mathbf{L}_h\widehat{\mathbf{U}}_{m,n},$$

where the matrix $\mathbf{L}_h$, the DG spatial operator, is defined as:

$$\mathbf{L}_h \equiv \mathbf{M}^{-1}(\mathbf{A} - \mathbf{B}_\pm\mathbf{e}^{\pm\mathrm{i}k_x m\Delta x} - \mathbf{C}_\pm\mathbf{e}^{\pm\mathrm{i}k_y n\Delta y}).$$

4.1. First-order RKDG method ($k = 1$)

The first-order RKDG method, which uses piecewise constants for the DG spatial discretization and the first-order forward Euler method in time, can be examined analytically. As an example, we consider the problem of propagation in the range $0 \leqslant \theta \leqslant \pi/2$ on the first grid pattern. For this case, the matrix $\mathbf{L}_h$ is given by:

$$\mathbf{L}_h = 2\|\mathbf{c}\|\frac{1}{\Delta x}\left\{\cos\theta\begin{bmatrix}-1 & e^{-i\alpha}\\ 1 & -1\end{bmatrix} + \sin\theta\begin{bmatrix}-1 & e^{-i\beta}\\ 1 & -1\end{bmatrix}\right\},$$

where $\alpha \equiv k_x m\Delta x$, $\beta \equiv k_y n\Delta y \in [0, 2\pi]$ (note $\Delta x = \Delta y$ for grid pattern I). It is a simple matter to verify that this is a normal matrix so condition (7) is necessary and sufficient for stability. We explicitly compute the eigenvalues of $\mathbf{L}_h$:

$$\lambda_\pm = -2\|\mathbf{c}\|\frac{1}{\Delta x}\left[\Theta \pm \sqrt{\Theta(\Theta_c - i\Theta_s)}\right],$$

where

$$\Theta \equiv \cos\theta + \sin\theta$$
$$\Theta_c \equiv \cos\theta\cos\alpha + \sin\theta\cos\beta$$
$$\Theta_s \equiv \cos\theta\sin\alpha + \sin\theta\sin\beta.$$

The stability condition (6) must be satisified for $z = \Delta t\lambda_\pm$. The characteristic polynomial of the forward Euler method is simply $P_{1,1} = 1 + z$ and so, in this case, assuming the separation of $\lambda_\pm$ into real $\mathscr{R}e$ and imaginary $\mathscr{I}m$ parts, condition (6) reads:

$$|P_{1,1}(z)|^2 = 1 + v[2\mathscr{R}e(\Lambda_\pm) + v(\mathscr{R}e(\Lambda_\pm)^2 + \mathscr{I}m(\Lambda_\pm)^2)] \leqslant 1, \tag{9}$$

where $\Lambda_\pm \equiv \lambda_\pm\Delta x/\|c\|$ and v is the Courant number (in two-dimensions we are initially defining this as $v = c\Delta t/\Delta x$). Assuming that both $\mathscr{R}e(\Lambda_\pm)\neq 0$ and $\mathscr{I}m(\Lambda_\pm)\neq 0$, inequality (9) can only be satisfied for $v > 0$ provided:

$$v \leqslant \bar{v} \equiv \frac{-2\mathscr{R}e(\Lambda_\pm)}{\mathscr{R}e(\Lambda_\pm)^2 + \mathscr{I}m(\Lambda_\pm)^2}. \tag{10}$$

With the help of the following identity for the square root of a complex number (see, for example, [21]):

$$\sqrt{x + iy} = \frac{\sqrt{2}}{2}\sqrt{\sqrt{x^2+y^2} + x} + i\,\mathrm{sgn}(y)\frac{\sqrt{2}}{2}\sqrt{\sqrt{x^2+y^2} - x},$$

the left side of (10) can be written in the form:

$$\bar{v} = \frac{1}{2\Theta}\left\{\frac{\mathscr{R}e(\Lambda_\pm)}{\mathscr{R}e(\Lambda_\pm) + (\Theta - \sqrt{\Theta_c^2 + \Theta_s^2})}\right\},$$

where

$$\mathscr{R}e(\Lambda_\pm) = -\left[2\Theta \pm \sqrt{2\Theta(\sqrt{\Theta_c^2 + \Theta_s^2} + \Theta_c)}\right].$$

It can be shown that $\mathscr{R}e(\Lambda_\pm) \leqslant 0$ and that $0 \leqslant \Theta - \sqrt{\Theta_c^2 + \Theta_s^2} \leqslant -\mathscr{R}e(\Lambda_\pm)$. Thus, $\bar{v}$ has a minimum value of $1/2\Theta$ over the range of all α and β, and the condition for stability is simply:

$$v \leqslant \bar{v} = \frac{1}{2\Theta}.$$

Recall that this expression is valid for directions of propagation $0 \leqslant \theta \leqslant \pi/2$ on grid pattern I, which corresponds to $1 \leqslant \Theta \leqslant \sqrt{2}$. In this range, the stability condition is most restrictive at $\theta = \pi/4$, in which case $v \leqslant \sqrt{2}/4$, and least restrictive at $\theta = 0$ and $\pi/2$ when the direction of propagation is along the shorter element edges, in which case $v \leqslant 1/2$.

Stability conditions for the full spectrum of propagation directions for grid patterns I and II can be derived in an analogous manner. Due to symmetry of the grids, stability conditions only need to be evaluated in the range $0 \leqslant \theta < \theta_*$ where $\theta_* = \pi$ for grid pattern I and $\theta_* = \pi/3$ for grid pattern II. These conditions are plotted in Fig. 5 as functions of θ. Note that for grid pattern I, the stability condition in the full range of propagation is least restrictive at $\theta = 3\pi/4$, when the direction of propagation is parallel to the longest element edge. In fact, this condition, $v \leqslant 1/\sqrt{2}$, corresponds to the well-known two-dimensional CFL condition for a finite difference scheme on a rectilinear grid. We elaborate on this in Section 4.3. Similarly, for grid pattern II, the stability condition is least restrictive, in this case $v \leqslant 1/2$, when the direction of propagation is parallel to the element edges. The most restrictive conditions are $v \leqslant \sqrt{2}/4$ and $v \leqslant \sqrt{3}/4$ at $\theta = \pi/4$ and $\theta = \pi/6$ for grid patterns I and II, respectively. These extremum conditions, denoted $\bar{v}_{\min}$ and $\bar{v}_{\max}$, are summarized in Table 1 along with the condition for propagation for $\theta = 0$, denoted $\bar{v}_0$. Finally, we note that the stability condition for a given RK method applied to the $p = 0$ DG spatial discretization is given by the SSP theorem since for this case the forward Euler method is stable for a given Courant number.

4.2. Higher-order RKDG methods ($k \geqslant 2$)

In this section, we examine the higher-order RKDG cases. As in the $k = 1$ case, we explicitly compute the form of the DG spatial operators $\mathbf{L}_h$. Following the approach outlined earlier in this section, this is a straightforward process. The eigenvalues

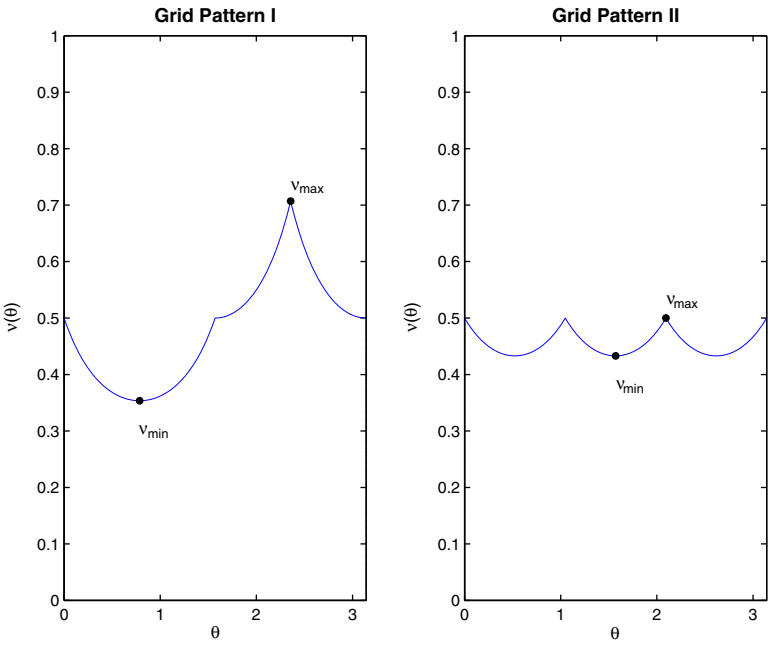

Fig. 5. The stability conditions as a function θ for grid patterns I and II.

Table 1
Stability conditions for the first-order RKDG method

Grid pattern	$\bar{\nu}_0$	$\bar{\nu}_{\min}, \theta_{\min}$	$\bar{\nu}_{\max}, \theta_{\max}$
I	$\frac{1}{2}$	$\frac{\sqrt{2}}{4}, \frac{\pi}{4}$	$\frac{1}{\sqrt{2}}, \frac{3\pi}{4}$
II	$\frac{1}{2}$	$\frac{\sqrt{3}}{4}, \frac{\pi}{6}$	$\frac{1}{2}, \frac{\pi}{3}$

of these matrices are then computed numerically at a discrete number of points for $\alpha, \beta \in [0, 2\pi]$ for a given ν, which is increased incrementally until the stability condition is violated.

We summarize the results found using this approach for second-, third-, and fourth-order RKDG methods on grid patterns I and II in Table 2. In each case, we investigate the use of SSP (s,k) RK methods with up to $s = 8$. As with the first-order RKDG method, we report the values of $\bar{\nu}_{\min}$ and $\bar{\nu}_{\max}$. (We implicitly assume that the minimum and maximum constraints on the Courant number occur at the same directions of wave propagation as for the first-order case. As will be seen, this is not strictly the case.) Additionally, we report the relative cost Γ of the various RKDG methods using the $s > k$ RK methods compared to the RKDG method using the RK method with non-negative coefficients that has the minimum number of stages $s_{\min}$ required for a given order (note that $s_{\min} = k$ for $k = 2$ and 3, however, for $k = 4$, $s_{\min} = 5$; see [12]). These values are computed based on the values of $\bar{\nu}_{\min}$. For example, while the SSP (3,2) RKDG method, which is found to be the optimal second-order RKDG method, allows a time step roughly 1.85 times that of the SSP (2,2) RKDG method it requires one additional evaluation of F. Thus, a given time T can be reached (assuming the maximum allowable time step is used) at approximately 80% of the computational cost of the SSP (2,2) RKDG method. The optimal third-order method is achieved using the SSP (7,3) RK method although its efficiency is only marginally better than that of the SSP (5,3) method and requires more storage. Thus, in practice, the SSP (5,3) would most likely be more efficient. For the fourth-order RKDG methods, all of the $s > 5$ RK methods offer roughly the same moderate savings over the SSP (5,4) RK method.

It is interesting to note that the increases observed in the CFL conditions for linear stability by using additional stages are not as great as the corresponding increases observed in the CFL conditions for TV-stability (or enforcement of a maximum principle), which are a function of κ of Theorem 1. For example, κ increases by a factor of 2 in going from the SSP (2,2) RK method to the SSP (3,2) RK method; however, the corresponding CFL condition for linear stability only increases by a factor of about 1.7 (for $\bar{\nu}_{\max}$).

From these results, it can also be observed that the differences between $\bar{\nu}_{\min}$ and $\bar{\nu}_{\max}$ generally become less significant as both p and s are increased. For example, the ratio of $\bar{\nu}_{\min}$ to $\bar{\nu}_{\max}$ for the first-order RKDG method on grid patterns I and II are 0.5 and $0.866 (\approx \sqrt{3}/2)$, respectively, while for the higher-order methods, these ratios are 0.525 and 0.910, 0.527 and 0.913, and 0.558 and 0.967 for the SSP (2,2), SSP (3,3), and SSP (5,4) RKDG methods, respectively. As an example of this trend with respect to the number of stages for a fixed value of p, it can be noted that for grid pattern II the ratio of $\bar{\nu}_{\min}$ to $\bar{\nu}_{\max}$ is 0.910 for

Table 2
Two-dimensional CFL conditions and relative cost of the SSP (s,k) RKDG methods

Stages, s	SSP $(s,2)$			SSP $(s,3)$			SSP $(s,4)$		
	$\bar{\nu}_{\min}$	$\bar{\nu}_{\max}$	Γ	$\bar{\nu}_{\min}$	$\bar{\nu}_{\max}$	Γ	$\bar{\nu}_{\min}$	$\bar{\nu}_{\max}$	Γ
Grid pattern I									
2	0.1730	0.3292	–	–	–	–	–	–	–
3	0.3205	0.5658	0.81	0.1225	0.2324	–	–	–	–
4	0.4150	0.7447	0.83	0.1850	0.3296	0.88	–	–	–
5	0.4901	0.8874	0.88	0.2502	0.4320	0.82	0.1319	0.2490	–
6	0.5533	1.0061	0.94	0.3002	0.5134	0.82	0.1792	0.3102	0.88
7	0.6077	1.1076	1.00	0.3521	0.5999	0.81	0.2100	0.3597	0.88
8	0.6557	1.1965	1.06	0.4004	0.6817	0.82	0.2424	0.4120	0.88
Grid pattern II									
2	0.2119	0.2328	–	–	–	–	–	–	–
3	0.3925	0.4001	0.81	0.1500	0.1643	–	–	–	–
4	0.5083	0.5266	0.83	0.2266	0.2330	0.88	–	–	–
5	0.6003	0.6275	0.88	0.3065	0.3054	0.82	0.1702	0.1761	–
6	0.6776	0.7114	0.94	0.3676	0.3630	0.82	0.2195	0.2193	0.93
7	0.7443	0.7832	1.00	0.4312	0.4242	0.81	0.2572	0.2544	0.93
8	0.8031	0.8461	1.06	0.4904	0.4820	0.82	0.2969	0.2913	0.92

the SSP (2,2) RKDG method and 0.949 for the SSP (8,2) method. In fact, on grid pattern II it can be noted that for the third-order RKDG methods with $s > 5$ and the fourth-order methods with $s > 6$ the $\bar{\nu}_{\min}$ are actually found to be slightly greater (though by <2%) than the $\bar{\nu}_{\max}$.

4.3. Relation to one-dimension CFL conditions

It is interesting to attempt to relate these two-dimensional CFL conditions to the one-dimensional conditions derived in [7,15] by defining a Courant number in terms of an appropriately defined grid parameter or "element diameter" h. Here, we have initially taken h to be the shortest element edge, i.e. $h \equiv \Delta x$. Indeed, such an approach is often used in practice to select an appropriate time step (see, for example, [1,8,19]), i.e.

$$\Delta t \leqslant \frac{h}{\|\mathbf{c}\|}\bar{\nu}_{1D}, \tag{11}$$

where $\bar{\nu}_{1D}$ is the maximum Courant number that can be used in one-dimension.

To this end, first it can be observed that the stability conditions plotted in Fig. 5 have the same form as a plot of the length of the chord $r(\theta)$ drawn from a vertex to the perimeter of the "stencil" of elements that surround that vertex; see Fig. 6. Thus, if one defines a direction-dependent grid parameter $h_\theta = r(\theta)$ then for a given direction of wave propagation θ the two-dimensional CFL conditions for the first-order RKDG method can be expressed in terms of h_θ and the one-dimensional CFL condition simply as:

$$p = 0: \ \|\mathbf{c}\|\frac{\Delta t}{h_\theta} \leqslant \frac{1}{2}\bar{\nu}_{1D}. \tag{12}$$

Obviously, if a time step is to be selected that will be stable for wave propagation in an arbitrary direction then one must take:

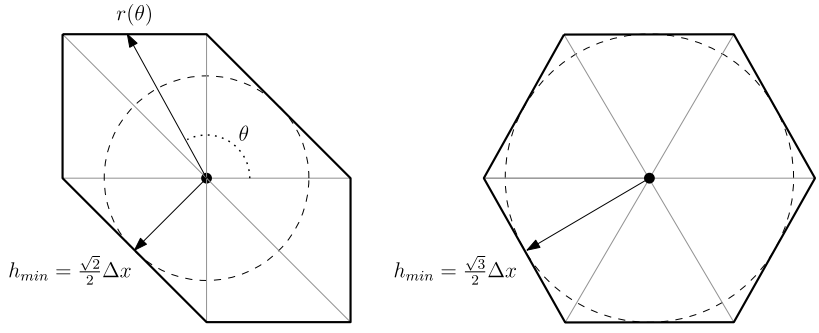

Fig. 6. The distance $r(\theta)$ used to define an appropriate mesh spacing parameter h for triangular grids.

$$p = 0: \ \Delta t \leqslant \frac{1}{2}\frac{h_{\min}}{\|\mathbf{c}\|}, \tag{13}$$

where $h_{\min}$ is the radius of the largest circle that is entirely contained within the stencil of elements surrounding a vertex (see Fig. 6) and where we have used the fact that $\bar{\nu}_{1D} = 1$ for the first-order RKDG method. We remark that this definition of $h_{\min}$ has an obvious relation to the two-dimensional CFL condition for a finite difference method on a rectilinear grid – namely, that the domain of dependence of a finite difference grid point, which is a spherical cone in two-dimensions, must be contained within the finite difference stencil; see [10]. Note that condition (13), which is necessary and sufficient for stability, is stricter than using condition (11) with h defined as the shortest element edge or the diameter of the inscribed circle of the element – two approaches that are commonly used in practice.

This simple result, however, does not hold for the higher-order RKDG methods. However, for the second-order RKDG methods, it can be observed that if the factor of 1/2 of condition (12) is replaced by $1/\sqrt{2}$ then one obtains a good approximation of the two-dimensional CFL conditions reported in Table 2 in terms of their one-dimensional counterparts. This leads us to consider the general condition:

$$\|\mathbf{c}\|\frac{\Delta t}{h_\theta} \leqslant \frac{1}{2^{1/(p+1)}}\bar{\nu}_{1D}. \tag{14}$$

Of course, for $p = 0$ we recover condition (11), which is an exact relation for the two-dimensional CFL conditions expressed in terms of the one-dimensional results. For $p = 1$, the estimates provided by (14) for $\bar{\nu}_{\max}$ are generally within 2% of those reported in Table 2 for both grid patterns I and II (the only exception being the SSP (3,2) method, which is within 4%). For $p = 2$ and $p = 3$, these estimates are within 7% for grid pattern I and 5% for grid pattern II. The estimates for $\bar{\nu}_{\min}$ provided by (14) are less accurate – though they are still within 10% of the computed values, with the errors increasing with the number of stages.

5. Numerical results

In this section, we verify the various stability conditions obtained in the previous section. We consider an initial condition given by a two-dimensional Gaussian function of the form:

$$u_0(x,y) = \frac{A}{2\pi\sigma}e^{-(x^2+y^2)/2\sigma^2}, \tag{15}$$

where A and σ are positive constants (see Fig. 7). Periodic boundary conditions are used, and we consider the two grid configurations of Fig. 3 with $\Delta y = 0.08$. To examine wave propagation in the directions corresponding to $\bar{\nu}_{\min}$ and $\bar{\nu}_{\max}$ for each grid pattern, we rotate the grid patterns and define the boundaries accordingly. For example, the conditions for $\bar{\nu}_{\max}$ are examined using the grids shown in Fig. 8(a) and (b) by taking $\mathbf{c} = (1,0)$ in Eq. (2).

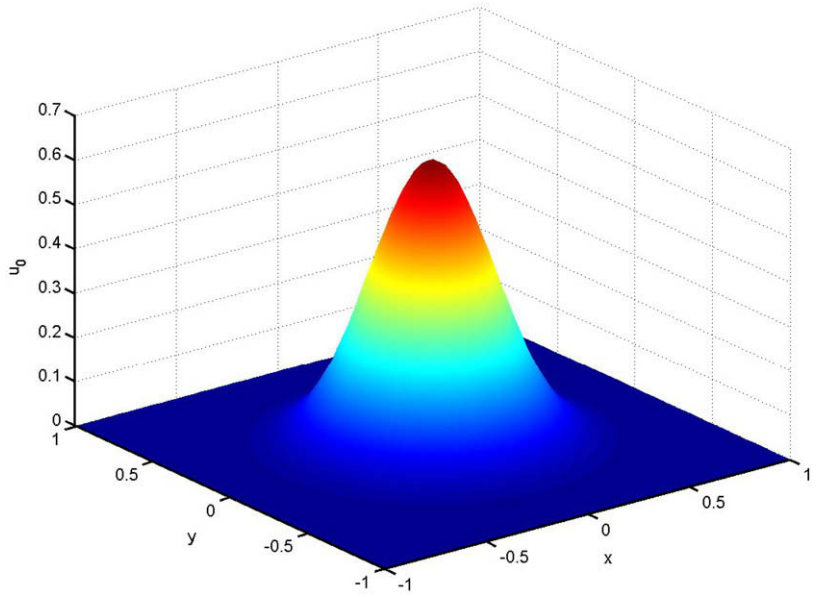

Fig. 7. The initial condition used for the numerical test.

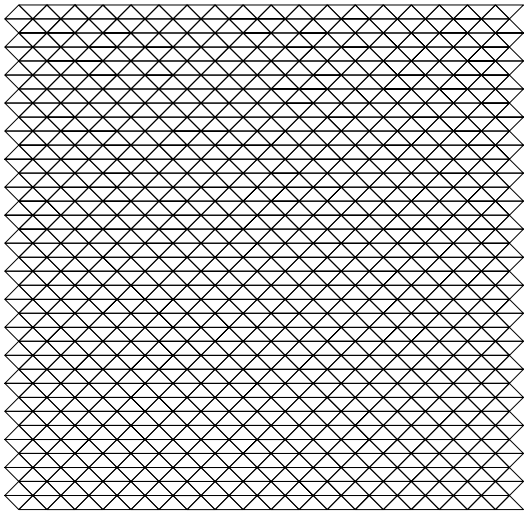

(a) Grid Pattern I

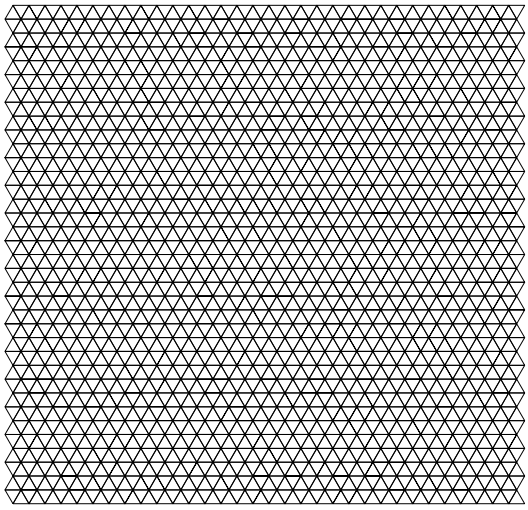

(b) Grid Pattern II

Fig. 8. Rotated grid patterns that are used to verify the the values of v_{max}.

Simulations are generally run for 20,000 time steps. The initial time step size that is used for a given simulation is determined by multiplying the corresponding $\bar{v}$ value obtained in the previous section by Δx. We then increase/decrease the time step accordingly such that the Courant number increases/decreases by 0.0001 until the code is unstable/stable. We report the largest values of v that give stable runs denoted $\hat{v}_{min}$ and $\hat{v}_{max}$. These conditions are summarized in Table 3 where we also report the absolute value of the relative errors E between the $\hat{v}_{min}$ and the theoretical results. As can be seen, excellent agreement is obtained between the values obtained from the stability analysis and those that can be used in practice. The numerical results are generally within 0.1% of the results obtained from the stability analysis. The first-order results (not shown in the Table 3) agree with the theoretical results derived in Section 4.1 to four decimal places.

6. Summary and conclusions

In this paper, we have derived CFL conditions for two-dimensional RKDG methods on triangular grids. Two structured grid configurations were analyzed, and wave propagation in different directions was considered. Necessary and sufficient conditions for stability were derived analytically for the first-order RKDG method, and necessary conditions, which also appear to be sufficient, were found for the higher-order cases. With an appropriately defined grid parameter h these conditions were found to be, in general, approximately equal to the one-dimensional CFL conditions found in [6,15] times a factor that is

Table 3
Numerical CFL estimates of the SSP (s,k) RKDG methods and relative errors (in %) from the theoretical results

Stages, s	SSP $(s,2)$			SSP $(s,3)$			SSP $(s,4)$		
	$\hat{\nu}_{\min}$	$\hat{\nu}_{\max}$	$\lvert E \rvert$	$\hat{\nu}_{\min}$	$\hat{\nu}_{\max}$	$\lvert E \rvert$	$\hat{\nu}_{\min}$	$\hat{\nu}_{\max}$	$\lvert E \rvert$
Grid pattern I									
2	0.1731	0.3295	0.06	–	–	–	–	–	–
3	0.3207	0.5662	0.06	0.1225	0.2324	0.00	–	–	–
4	0.4153	0.7449	0.07	0.1851	0.3296	0.43	–	–	–
5	0.4906	0.8882	0.10	0.2503	0.4322	0.04	0.1391	0.2492	0.07
6	0.5537	1.0070	0.07	0.3004	0.5143	0.07	0.1793	0.3104	0.06
7	0.6083	1.1099	0.10	0.3523	0.6004	0.06	0.2101	0.3599	0.05
8	0.6565	1.2100	0.12	0.4008	0.6827	0.10	0.2425	0.4121	0.04
Grid pattern II									
2	0.2077	0.2328	2.00	–	–	–	–	–	–
3	0.3926	0.4002	0.03	0.1484	0.1644	1.07	–	–	–
4	0.5085	0.5267	0.04	0.2260	0.2331	0.26	–	–	–
5	0.6006	0.6276	0.05	0.3066	0.3056	0.03	0.1663	0.1761	2.29
6	0.6779	0.7115	0.04	0.3679	0.3633	0.08	0.2196	0.2194	0.05
7	0.7447	0.7834	0.05	0.4314	0.4244	0.05	0.2573	0.2544	0.04
8	0.8036	0.8463	0.06	0.4909	0.4822	0.10	0.2970	0.2913	0.03

a function of the degree of the DG spatial approximation p. The observed relationship between the one- and two-dimensional CFL conditions is exact for the first-order case and provides a good approximation of the conditions for higher-order RKDG methods. As was found to be in the case in one-dimension, optimal, in terms of computational efficiency, two-dimensional RKDG methods are obtained by using one or two additional stages than theoretically required for a given order. The computational savings achieved by using the $s > k$ RK methods in two-dimensions are moderately better than those observed in the one-dimensional case. The derived CFL conditions were verified on numerical examples.

Finally, although the CFL conditions were derived on structured grids, they could also serve as reasonable estimates for unstructured grids with h being defined analogously to what is depicted in Fig. 6. Additionally, based on the results found here, one can conjecture that the CFL conditions for RKDG methods on n-dimensional simplexes are given by a relation of the form:

$$\|\mathbf{c}\|\frac{\Delta t}{h} \leqslant \frac{1}{n^{f(p)}}\bar{\nu}_{1D}, \tag{16}$$

where h is a grid parameter defined analogously to the two-dimensional case considered here. This will be investigated in future work.

Acknowledgments

This work was supported by National Science Foundation Grants DMS 0620697 and 0620696 and by the Office of Naval Research, Award Number: N00014-06-1-0285.

References

[1] V. Aizinger, C. Dawson, A discontinuous Galerkin method for two-dimensional flow and transport in shallow water, Advances in Water Resources 25 (2002) 67–84.
[2] V. Aizinger, C. Dawson, B. Cockburn, P. Castillo, The local discontinuous Galerkin method for contaminant transport, Advances in Water Resources 24 (2001) 73–87.
[3] J.C. Butcher, The Numerical Analysis of Ordinary Differential Equations: Runge–Kutta and General Linear Methods, John Wiley, Chichester, 1987.
[4] G. Chavent, B. Cockburn, The local projection $P^0 - P^1$-discontinuous-Galerkin finite element method for scalar conservation laws, Mathematical Modelling and Numerical Analysis 23 (1989) 565–592.
[5] M.H. Chen, B. Cockburn, F. Reitich, High-order RKDG methods for computational electromagnetics, Journal of Scientific Computing 22 & 23 (2005) 205–226.
[6] B. Cockburn, C.W. Shu, TVB Runge–Kutta local projection discontinuous Galerkin finite element method for scalar conservation laws II: general framework, Mathematics of Computation 52 (1989) 411–435.
[7] B. Cockburn, C.W. Shu, The Runge–Kutta local projection P^1-discontinuous-Galerkin finite element method for scalar conservation laws, Mathematical Modelling and Numerical Analysis 25 (1991) 337–361.
[8] B. Cockburn, S. Hou, C.W. Shu, The Runge–Kutta discontinuous Galerkin method for conservation laws V: multidimensional systems, Journal of Computational Physics 141 (1998) 199–224.
[9] B. Cockburn, C.W. Shu, Runge–Kutta discontinuous Galerkin methods for convection dominated problems, Journal of Scientific Computing 16 (2001) 173–261.
[10] R. Courant, K. Friedrichs, H. Lewy, On the partial difference equations of mathematical physics, Mathematische Annalen 100 (1928) 32–74.
[11] J. Goodman, R. LeVeque, On the accuracy of stable schemes for 2D scalar conservation laws, Mathematics of Computation 45 (1985) 15–21.
[12] S. Gottlieb, C.W. Shu, Total variation diminishing Runge–Kutta schemes, Mathematics of Computation 67 (1998) 73–85.
[13] S. Gottlieb, C.W. Shu, E. Tadmor, Strong stability-preserving high-order time discretization methods, SIAM Review 43 (2001) 89–112.
[14] E.J. Kubatko, J.J. Westerink, C. Dawson, hp discontinuous Galerkin methods for advection dominated problems in shallow water flow, Computer Methods in Applied Mechanics and Engineering 196 (2006) 437–451.

[15] E.J. Kubatko, J.J. Westerink, C. Dawson, Semidiscrete discontinuous Galerkin methods and stage-exceeding-order, strong-stability-preserving Runge–Kutta time discretizations, Journal of Computational Physics 222 (2007) 832–848.
[16] S.C. Reddy, L.N. Trefethen, Stability of the method of lines, Numerische Mathematik 62 (1992) 235–267.
[17] R.D. Richtmyer, K.W. Morton, Difference Methods for Initial-Value Problems, 2nd ed., John Wiley, New York, 1967.
[18] S.J. Ruuth, Global optimization of explicit strong-stability-preserving Runge–Kutta methods, Mathematics of Computation 75 (2006) 183–207.
[19] D. Srmny, M.A. Botchev, J.J.W. van der Vegt, Dispersion and dissipation error in high-order Runge–Kutta discontinuous Galerkin discretisations of the Maxwell equations, Journal of Scientific Computing 33 (2007) 47–74.
[20] C.W. Shu, S. Osher, Efficient implementation of essentially non-oscillatory shock-capturing schemes, Journal of Computational Physics 77 (1988) 439–471.
[21] J. Spanier, K.B. Oldham, An Atlas of Functions, Hemisphere, Washington, DC, 1987.
[22] G. Strang, Linear Algebra and its Applications, Academic Press, New York, 1970.